Statistical Analysis of the Reaction-Zone Characteristics of Unstable Gaseous Detonations

XiaoCheng Mi
Laboratory for Scientific Computing, Cavendish Laboratory, University of Cambridge
Cambridge, United Kingdom

1 Introduction

There is a substantial collection of experimental evidence revealing that gaseous detonations consist of a multidimensional wave complex coupled with a spatially non-uniform release of chemical energy. These highly coupled wave and reaction dynamics determine the propagation behavior of gaseous detonation waves, such as the propagation limit in the presence of losses. Various experimental studies have demonstrated that detonations in highly unstable mixtures, i.e., those with a greater activation energy E_{a}, are more resilient to losses than those in weakly unstable mixtures. [1–3] Numerical simulation results based upon modeling an inviscid flow (described by the Euler equations), however, indicate that detonations governed by a greater E_{a} are more vulnerable to losses, which contradict the experimental findings. [2–5]

An explanation to reconcile these paradoxical findings has been conjectured: Within a highly unstable detonation complex, the combustion of a significant proportion of the reactive gases is governed by diffusive processes, rather than a shock-induced ignition; the Euler equations for an inviscid flow are thus inadequate to describe such diffusion-controlled combustion processes. [3] If this conjecture is true, refining the computational grid of a simulation based on the Euler equations would reduce the effect of numerical diffusion, and thus, impedes the energy release of a highly unstable mixture, resulting in a less resilient detonation to losses. In order to verify this conjecture, it is necessary to quantitatively examine the detailed spatial distribution of reaction rate within an unstable detonation wave complex. Using a combination of schlieren photographs and planar laser-induced fluorescence of OH radical, more detailed features of the reaction-zone structure of gaseous detonations have been revealed. [6–9] To experimentally obtain quantitative information on the spatial distribution of reaction rate, however, remains challenging. Since the complete flow-field data of gaseous detonations can be obtained via computational simulations, it is possible to perform more in-depth analysis on numerical results.

In this study, a framework of statistical analysis is proposed and performed to describe the reaction-zone characteristics of unstable gaseous detonations. The probability of the occurrence of a certain amount of gas reacting at a rate $\dot{\omega}$ and a distance relative to the location of the leading shock front is calculated. The

Correspondence to: xcm20@cam.ac.uk

probability functions of reaction rate resulting from two-dimensional simulations are compared with those of the corresponding ZND solutions. The objective of this study is to probe the diffusive effects on the statistical nature of the detonation reaction-zone dynamics. The effective diffusivity in the simulations can be varied via changing the physical diffusivity in a model based on the Navier-Stokes equations or refining the computational grid of an Euler-equations-based simulation. In this abstract, only the results of the simulations based on the Euler equations are presented.

2 Problem description

The reactive system consists of an inviscid, calorically perfect gas (i.e., with a constant ratio of specific heat γ). The gasdynamics of this system is described by the two-dimensional reactive Euler equations with flow and state variables non-dimensionalized with respect to the pre-shock, initial state. In this study, the reaction rate $\dot{\omega}$ is governed by single-step Arrhenius chemical kinetics as follows,

$$\frac{\partial Z}{\partial t} = -\dot{\omega} = -kZ\mathrm{Exp}\left(-E_\mathrm{a}/T\right) \tag{1}$$

where Z is the dimensionless reaction progress variable that varies from 1 (unreacted) to 0 (completely reacted), k is the pre-exponential factor, and E_a is the activation energy non-dimensionalized with respect to the pre-shock, initial state. Five different values of activation energy, i.e., $E_\mathrm{a} = 10$, 20, 30, 40, and 50 with a dimensionless energy release $Q = 50$ and a ratio of specific heat capacities $\gamma = 1.2$ are considered in this study. For each E_a, a specific value of k is selected so that the half-reaction-zone length $l_{1/2}$ of the corresponding ZND wave profile is of unity length. A spatially second-order accurate MUSCL-Hancock scheme with an approximate HLLE solution to the inter-cell Riemann problem was utilized to solve the governing equations. This solver is implemented on a CUDA-enabled parallel-processing platform using general-purpose graphic processing units (GPGPUs). [5, 10, 11]

The computational domain is an 80×80 square. The simulations are performed in a wave-attached reference frame via imposing an inflow at the Chapman-Jouguet (C-J) velocity ($-D_\mathrm{CJ}$) along the right boundary of the domain. The detonation is initiated via the compression of a blast wave generated by a high-pressure zone initially placed in the flow. A two-dimensional, sinusoidal perturbation in density is introduced next to the initial high-pressure zone to facilitate the development of transverse instabilities. Statistical analysis is performed to the fully developed wave structure after the wave front has propagated over approximately 500 times the ZND half-reaction-zone length.

3 Sample results

Some sample numerical schlieren graphs for the cases with $E_\mathrm{a} = 20$ and 50 are shown in the first and second row of Fig. 1, respectively. Each column of Fig. 1 corresponds to the simulations at a specific numerical resolution. The cases with $E_\mathrm{a} = 20$ result in a typical wave structure of regular or weakly unstable detonations. A more irregular wave structure arises from the cases with $E_\mathrm{a} = 50$. Although finer features are captured near the leading shock front, the global wave structure for $E_\mathrm{a} = 20$ does not exhibit any significant change as the resolution is increased from 50 to 100 computational grid points per the ZND half-reaction-zone length. However, for $E_\mathrm{a} = 50$, larger pockets of slowly reacting gases indicated by the dark gray areas can be observed as the resolution is increased to $l_{1/2}/\Delta x = 100$.

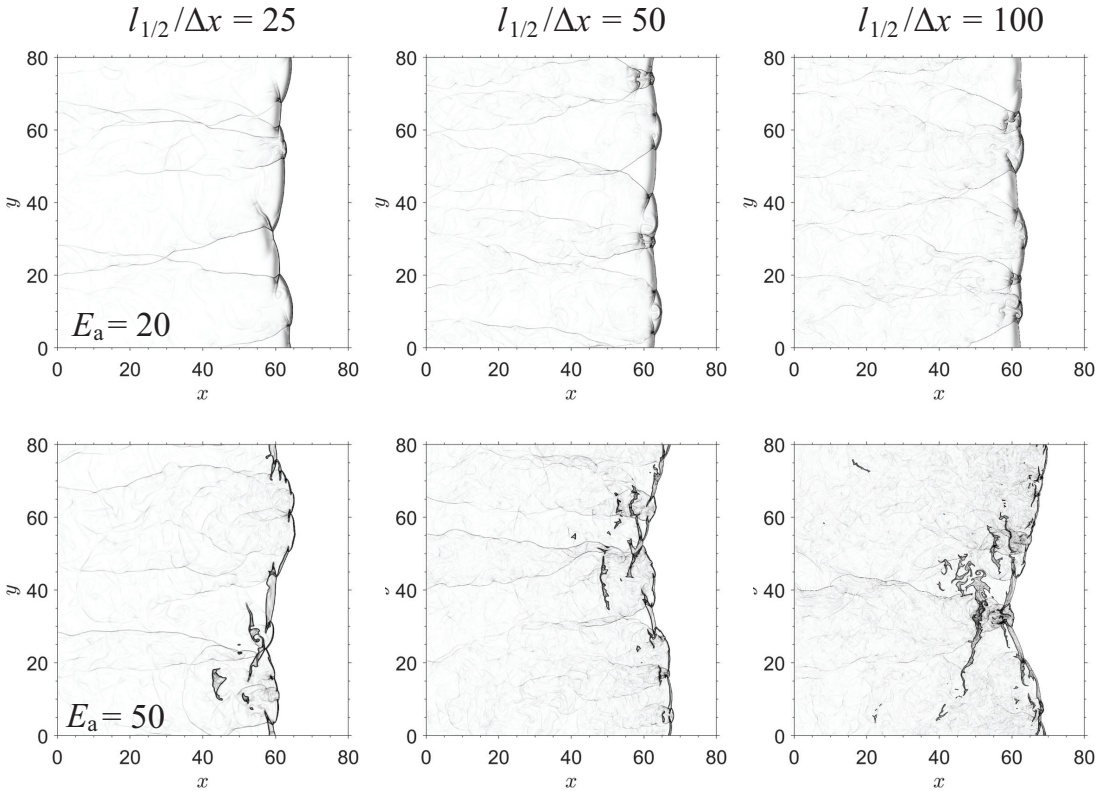

Figure 1: Sample simulation results of schlieren graphs for the cases with $E_\mathrm{a} = 20$ and 50 at numerical resolutions of 25, 50, and 100 computational grid points per the ZND half-reaction-zone length.

4 Statistical analysis

4.1 Methodology

To obtain the probability distribution, the probability mass for two variables, reaction rate $\dot{\omega}$ and location in the propagation direction of the detonation wave x, is counted. The range considered for each of these two variables are divided into discrete intervals (or "bins"). The indices for the discrete intervals of $\dot{\omega}$ and x are i and j, respectively. For a computational grid point at a position (X, Y), the local reaction rate $\dot{\omega}(X, Y)$ and X-coordinate falls into the bin of $\dot{\omega}_i$ and x_j if the following criteria are satisfied,

$$\log_{10}(\dot{\omega}_i) - \mathrm{d}\mathcal{E}/2 < \log_{10}(\dot{\omega}(X, Y)) \leq \log_{10}(\dot{\omega}_i) + \mathrm{d}\mathcal{E}/2 \tag{2}$$

$$x_j - \mathrm{d}x/2 < X \leq x_j + \mathrm{d}x/2 \tag{3}$$

where $\mathcal{E}$ is the exponent of the value of $\dot{\omega}(X, Y)$ on the basis of a decadic logarithm, i.e., $\dot{\omega}(X, Y) = 10^{\mathcal{E}}$, and $\mathrm{d}\mathcal{E}$ and $\mathrm{d}x$ represent the bin size of $\dot{\omega}$ and x, respectively. The occurrence of a data point to $\dot{\omega}_i$ and x_j is counted with the weight of the remaining reactant at this point. Thus, the probability mass $m_{i,j}$ is counted as follows,

$$m_{i,j} = \sum_{k}^{N_{i,j}} \rho_k Z_k \tag{4}$$

where $N_{i,j}$ is the total number of data points that fall into the bin of $\dot{\omega}_i$, and x_j and k is the index of each of these data points. The total mass over the considered range of $\dot{\omega}$ and x can be calculated as follows,

$$M = \sum_i \sum_j m_{i,j} \tag{5}$$

The probability $P_{\mathrm{m}}(\dot{\omega}, x)$ and probability density function (p.d.f.) $f_{\mathrm{m}}(\dot{\omega}, x)$ can be calculated as follows,

$$P_{\mathrm{m}}(\dot{\omega}_i, x_j) = m_{i,j}/M \tag{6}$$

$$f_{\mathrm{m}}(\dot{\omega}_i, x_j) = P_{\mathrm{m}}(\dot{\omega}_i, x_j)/(\mathrm{d}\mathcal{E}\mathrm{d}x) \tag{7}$$

where subscript "m" denotes that the probability is weighted by the mass of the remaining reactant. According to the sum rule of probability functions, the probability and p.d.f. of only $\dot{\omega}$ can be obtained as follows,

$$P_{\mathrm{m}}(\dot{\omega}_i) = \sum_j P_{\mathrm{m}}(\dot{\omega}_i, x_j) \tag{8}$$

$$f_{\mathrm{m}}(\dot{\omega}_i) = P_{\mathrm{m}}(\dot{\omega}_i)/\mathrm{d}\mathcal{E} \tag{9}$$

Via detecting the position of the leading shock front in each snapshot collected over time, the p.d.f. of shock front position $f(x_{\mathrm{s}})$ can be obtained. Note that the p.d.f. of shock front position does not have to be weighted by the mass of reactant since the flow in front of the shock front is uniform—the material processed by the leading shock is of the same density.

4.2 Statistical results and discussion

The probability density functions $f_{\mathrm{m}}(\dot{\omega}, x)$ resulting from the two-dimensional simulations are shown as the upper subfigures of Fig. 2. The lower subfigures of Fig. 2 are the corresponding p.d.f of shock front position. For all of these three cases, the yellow regions in the contour plots of $f_{\mathrm{m}}(\dot{\omega}, x)$ are located within the vicinity of where the corresponding $f(x_{\mathrm{s}})$ peaks. For $E_{\mathrm{a}} = 10$, the significant reaction spans over a range of approximately $10^{-2} < \dot{\omega} < 10^{0}$; as E_{a} increases to 50, the significant reaction range in $\dot{\omega}$ expands to approximately $10^{-4} < \dot{\omega} < 10^{1}$. Note the simulation results analyzed in this section are obtained from the simulations with a resolution of $l_{1/2}/\Delta x = 50$.

The mass-weighted p.d.f. of only $\dot{\omega}$ for the simulation results with $E_{\mathrm{a}} = 10$, 30, and 50 are shown in Fig. 3. The gray curves are the $f_{\mathrm{m}}(\dot{\omega})$ based on a snapshot of the flow field at a specific time, and the orange curve is the $f_{\mathrm{m}}(\dot{\omega})$ averaged over a period of 30 units of time, which comprises 150 snapshots with an equal interval of 0.2 unit of time. The blue curves are the corresponding $f_{\mathrm{m}}(\dot{\omega})$ for the ZND solution. For $E_{\mathrm{a}} = 10$, the p.d.f. corresponding to each snapshot is very close to the time-averaged p.d.f.; the p.d.f. resulting from the simulations spans over approximately the same range of reaction rate as that of the ZND solution does. As E_{a} increases, the p.d.f. of the snapshots significantly fluctuate around the time-averaged p.d.f., and the range of $\dot{\omega}$ covered the p.d.f. of the simulation data is boarder than that covered by the ZND solution. For the case with $E_{\mathrm{a}} = 50$, the peak of $f_{\mathrm{m}}(\dot{\omega})$—indicating at which rate the most of the material reacts—is smaller than that of the ZND solution by one order of magnitude. This statistical results provide a quantitative measurement of how much material undergoes a significantly slow reaction. How the statistical behavior of slow reaction is affected by the artificial or physical diffusivities will be examined within the complete scope of this study.

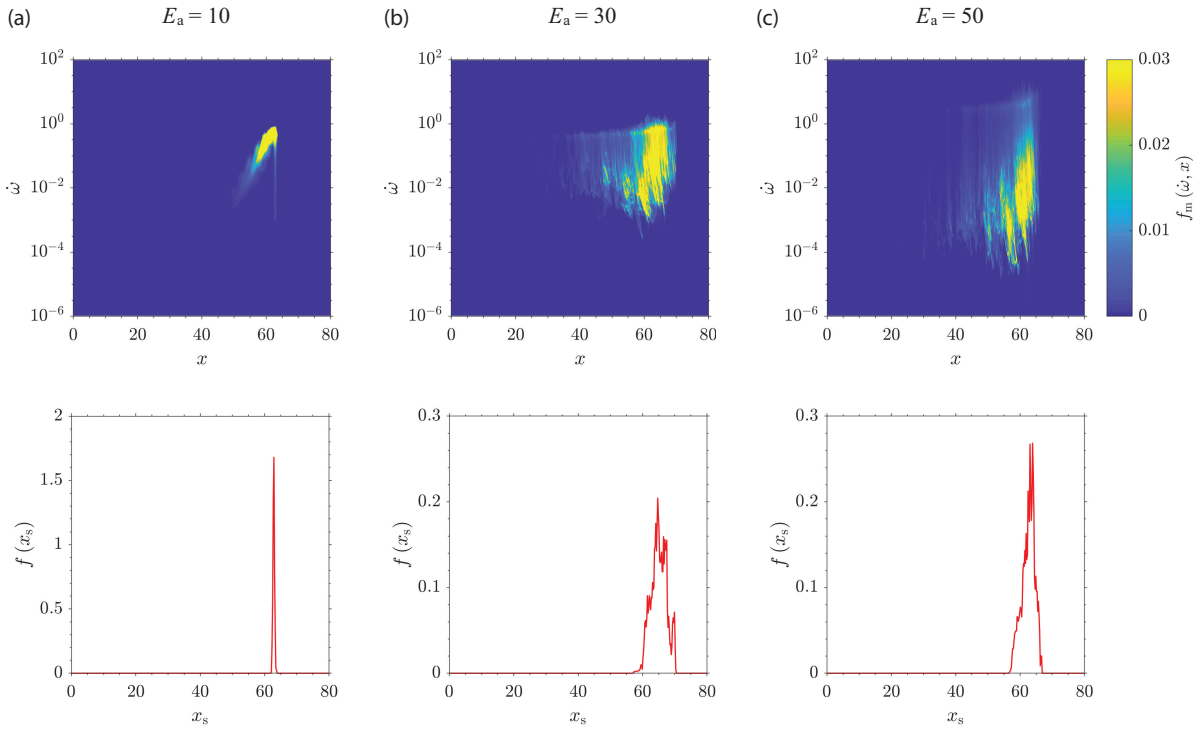

Figure 2: The statistical results for the simulation data with $E_a = 10$, 30, and 50: (upper row) the reactant-mass-weighted probability density function of reaction rate and position in the propagation direction of the detonation wave, i.e., $f_m(\dot{\omega}, x)$; (lower row) the p.d.f. of shock front position, i.e., $f(x_s)$.

5 Concluding remarks

A framework of methodology to probe the statistical characteristics of the reaction-zone dynamics arising from two-dimensional unstable detonations has been proposed in this study. Via this statistical analysis, the probability distribution of various reaction rates that the reactive material undergoes within a detonation wave complex can be quantitatively measured and presented. This analysis will be used to gain further insights into the governing combustion mechanisms of unstable gaseous detonations.

References

[1] M. Radulescu and J. Lee, "The failure mechanism of gaseous detonations: experiments in porous wall tubes," *Combustion and Flame*, vol. 131, no. 12, pp. 29 – 46, 2002.

[2] M. Radulescu and B. Borzou, "Dynamics of detonations with a constant mean flow divergence," *Journal of Fluid Mechanics*, vol. 845, p. 346377, 2018.

[3] M. Radulescu, "A detonation paradox: Why inviscid detonation simulations predict the incorrect trend for the role of instability in gaseous cellular detonations?" *Combustion and Flame*, vol. 195, pp. 151 – 162, 2018.

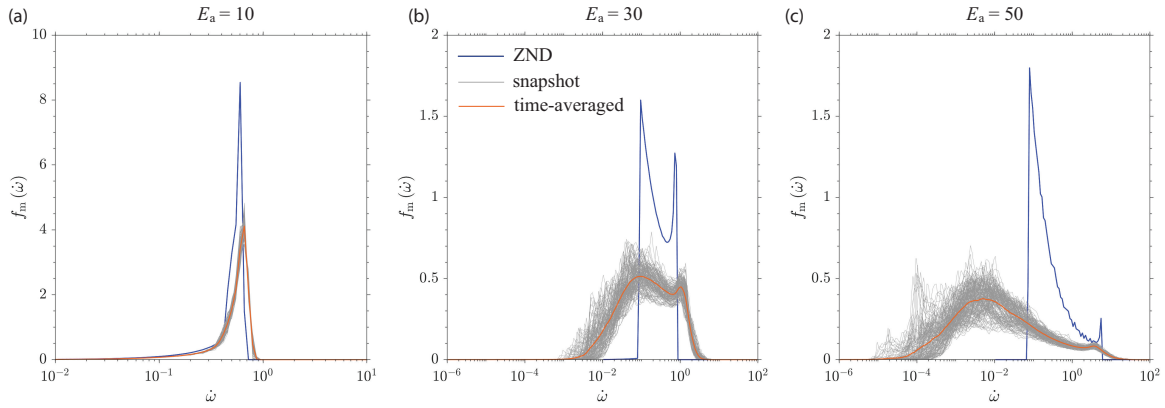

Figure 3: The reactant-mass-weighted probability density function of reaction rate, i.e., $f_{\mathrm{m}}(\dot{\omega})$, for the cases with $E_{\mathrm{a}} = 10$, 30, and 50.

[4] M. Reynaud, F. Virot, and A. Chinnayya, "A computational study of the interaction of gaseous detonations with a compressible layer," *Physics of Fluids*, vol. 29, no. 5, p. 056101, 2017.

[5] X. Mi, A. Higgins, C. Kiyanda, H. Ng, and N. Nikiforakis, "Effect of spatial inhomogeneities on detonation propagation with yielding confinement," *Shock Waves*, vol. 28, no. 5, pp. 993–1009, 2018.

[6] F. Pintgen, C. Eckett, J. Austin, and J. Shepherd, "Direct observations of reaction zone structure in propagating detonations," *Combustion and Flame*, vol. 133, no. 3, pp. 211 – 229, 2003.

[7] J. Austin, F. Pintgen, and J. Shepherd, "Reaction zones in highly unstable detonations," *Proceedings of the Combustion Institute*, vol. 30, no. 2, pp. 1849 – 1857, 2005.

[8] J. Shepherd, "Detonation in gases," *Proceedings of the Combustion Institute*, vol. 32, no. 1, pp. 83 – 98, 2009.

[9] C. Kiyanda and A. Higgins, "Photographic investigation into the mechanism of combustion in irregular detonation waves," *Shock Waves*, vol. 23, no. 2, pp. 115–130, 2013.

[10] C. Kiyanda, G. Morgan, N. Nikiforakis, and H. Ng, "High resolution gpu-based flow simulation of the gaseous methane-oxygen detonation structure," *Journal of Visualization*, vol. 18, no. 2, pp. 273–276, 2015.

[11] X. Mi, A. Higgins, H. Ng, C. Kiyanda, and N. Nikiforakis, "Propagation of gaseous detonation waves in a spatially inhomogeneous reactive medium," *Physical Review Fluids*, vol. 2, no. 5, p. 053201, 2017.